UNIVERSITY *of* York

This is a repository copy of *Representative Contents Design for Shielding Enclosure Qualification from 2 to 20 GHz*.

White Rose Research Online URL for this paper:
https://eprints.whiterose.ac.uk/id/eprint/116849/

Version: Accepted Version

White Rose
university consortium
Universities of Leeds, Sheffield & York

eprints@whiterose.ac.uk
https://eprints.whiterose.ac.uk/

# Representative Contents Design for Shielding Enclosure Qualification from 2 to 20 GHz

Ian D. Flintoft[1], Simon J. Bale[1] Andy C. Marvin[1], Ming Ye[2], John. F. Dawson[1], Changyong Wan[3], Mengze Zhang[3], Sarah L. Parker[1] and Martin P. Robinson[1]

[1] *Department of Electronics, University of York, Heslington, York YO10 5DD, UK*
[2] *Huawei Technologies AB, Research and Development Center, Box 54, SE-164, 94 Kista Sweden*
[3] *Huawei Technologies Co. Ltd., Global Compliance and Testing Center, Building F4, Huawei Industrial Base, Bantian Longgang, Shenzhen 518129, P. R. China*

# Representative Contents Design for Shielding Enclosure Qualification from 2 to 20 GHz

Ian D. Flintoft, *Senior Member, IEEE*, Simon J. Bale, *Member, IEEE,* Andy C. Marvin, *Fellow IEEE,* Ming Ye, John F. Dawson, *Member, IEEE,* Changyong Wan, Mengze Zhang, Sarah L. Parker and Martin P. Robinson, *Member, IEEE*

*Abstract*—**The electromagnetic environment inside a shielding enclosure is affected by the absorption characteristics of the contents, which should therefore be represented in shielding measurements and simulations. At frequencies up to a few gigahertz, lossy dielectric materials have previously been used as surrogates for printed circuit boards in enclosure shielding assessment, both experimentally and in simulations. However, no systematic methodology for the design of these surrogates and their calibration against real hardware at high frequencies has been elucidated. In this paper we show how both lossy dielectric material and microstrip transmission line based "representative contents" can be designed and calibrated against real printed circuit boards over the frequency range 2-20 GHz using power balance concepts. The calibration is made by matching the average absorption cross-section of the surrogate to an average value for a class of real contents measured in a reverberation chamber. The surrogates are designed using efficient power balance models for layered media and field-excited microstrip lines and verified using full-wave simulation. The fabricated surrogates are validated by shielding measurements. The methodology presented could form an important part of future standards for enclosure qualification measurements that more accurately represent the internal environment of real equipment.**

*Index Terms*—**shielding, printed circuit board, absorption cross-section, reverberation chamber, power balance**

## I. Introduction

Absorption in the contents of a shielding enclosure can have a big impact on the electromagnetic environment inside the enclosure and therefore on the radiated immunity and emissions of the equipment it comprises. The assessment of enclosure shielding effectiveness is usually carried out with an empty enclosure. Some work on modeling the effect of an enclosure's content on its shielding characteristics has been reported, mostly considering frequencies up to a few gigahertz [1], [2]. More recent work has shown how even the losses in enclosure walls impact on shielding performance at high frequencies [3], [4]. Proposals have been made to improve the relevance of shielding effectiveness (SE) metrics by incorporating loading into the enclosure during shielding measurements [5], [6]. IEEE Standard 299.1 contains an informative annex (Annex K) describing how to utilize absorbing materials in equipment enclosures for the measurement of shielding properties [7]. However, there are no detailed guidelines for achieving representative contents (ReCos) at high frequencies. Such generic ReCos are necessary for the development of a standardized assessment methodology for populated enclosure SE and the qualification of enclosures for particular environments and contents.

Power balance (PWB) analysis is an efficient method for estimating the average electromagnetic field inside electrically large enclosures. The method is described in detail in [8], [9] and a systematic application of the method to enclosure shielding is given in [10]. This analysis shows that the plane-wave absorption cross-section (ACS) of a printed circuit board (PCB) averaged over angles of arrival and polarizations of the incident plane-wave is the intrinsic property of a PCB that determines its loading effect on an enclosure and hence the perturbation in SE caused by the contents. Such an average ACS (AACS) can be measured in a reverberation chamber (RC) [11]. A database of measured AACSs for real PCBs taken from information and communication technology (ICT) equipment was reported in [10]; according to the PWB analysis such measured AACS data can be used to calibrate ReCos for SE measurements.

Here we propose two approaches to making ReCos that are surrogates for PCBs. The first, based on radio absorbing material (RAM), is an extension of earlier ideas from low frequency [12]. The second, using loaded microstrip transmission lines (TLs), is motivated by the fact that absorption in devices at the end of tracks is one of the important loss mechanisms in real PCBs; this approach may also be more appropriate for eventual standardization. In both cases the proposed ReCo designs are calibrated against real PCBs using the AACS as the matching criterion.

In Section II we summarize the PWB analysis of enclosure

I. D. Flintoft, S. J. Bale, A. C. Marvin, J. F. Dawson, S. L. Parker and M. P. Robinson are with the Department of Electronic Engineering, University of York, Heslington, York, YO10 5DD (e-mail: ian.flintoft@york.ac.uk, simon.bale@york.ac.uk, andy.marvin@york.ac.uk, john.dawson@york.ac.uk, slp504@york.ac.uk, martin.robinson@york.ac.uk).

Ming Ye is with Huawei Technologies AB, Research and Development Center, Box 54, SE-164, 94 Kista Sweden (email: ming.ye@huawei.com).

Changyong Wan and Mengze Zhang are with Huawei Technologies Co. Ltd., Global Compliance and Testing Center, Building F4, Huawei Industrial Base, Bantian Longgang, Shenzhen 518129, P. R. China (email: wanchangyong@huawei.com, zhangmengze@huawei.com,).

SE and detail the PWB models used to design both types of ReCos. The design and fabrication processes for the ReCos are described in Section III; the designs were verified using full-wave simulations that are described in Section IV. RC shielding measurements were used to validate the ReCos as described in Section V. The results of the simulations and measurements are presented in Section VI, leading to the conclusions in Section VII.

## II. POWER BALANCE MODELS

In the following we use $\langle \cdot \rangle$ to denote average values over an ensemble of systems, specifically the external and internal field distributions of an enclosure in an RC. We take it that the assumptions of the PWB method are valid; in particular, that the enclosure is electrically large, the contents are a least a quarter of a wavelength from the walls and the Q-factor is sufficiently high for a diffuse field to be established.

### A. RC shielding measurement

The SE of an enclosure in a reverberant environment is defined as the ratio of the average scalar power density outside, $\langle S_e \rangle$, to that inside, $\langle S_i \rangle$: $\langle SE \rangle \overset{\text{def}}{=} \langle S_e \rangle / \langle S_i \rangle$ [7]. In [10] and [12] it is shown that the SE for a populated enclosure is

$$\langle SE_{\text{populated}} \rangle = 1 + \frac{\langle \sigma^a_{\text{i;walls}} \rangle + \langle \sigma^a_{\text{i;contents}} \rangle}{\langle \sigma^t \rangle} \tag{1}$$

where $\langle \sigma^t \rangle$ is the total average transmission cross-section (ATCS) of the enclosure's apertures, $\langle \sigma^a_{\text{i;walls}} \rangle$ is the total AACS of the inside of the enclosure walls and $\langle \sigma^a_{\text{i;contents}} \rangle$ is the total AACS of the contents, including any antennas. This equation shows that both the total AACS of the contents and the total ATCS of the apertures directly determine the SE of the enclosure at high frequencies. We see that the SE of an empty enclosure, $\langle SE_{\text{empty}} \rangle$, is as much a measure of its wall losses as it is of the transmission through its apertures [3], [4]. Furthermore, considering the cases where the enclosure is either empty or populated we find [3], [10]

$$\langle SE_{\text{populated}} \rangle = \langle SE_{\text{empty}} \rangle + \frac{\langle \sigma^a_{\text{i;contents}} \rangle}{\langle \sigma^t \rangle} \tag{2}$$

which shows that knowledge of $\langle SE_{\text{empty}} \rangle$ is in itself insufficient for predicting the SE of a populated enclosure. Indeed, the ATCS of an enclosure is a much more useful metric as it allows the SE of a populated enclosure to be predicted from the AACS of the contents using (2), under the assumption that in practical cases $\langle \sigma^a_{\text{i;walls}} \rangle \ll \langle \sigma^a_{\text{i;contents}} \rangle$. If both the empty enclosure SE and the ATCS of an enclosure are known then populated SE can be predicted even if the wall losses are significant. This analysis also shows that providing the contents are replaced by a surrogate with the same average AACS, the SE will be unchanged. We therefore propose to use the AACS to design representative contents for populated enclosure shielding measurements.

### B. Determination of AACS

In the following sections we will calculate the AACS of specific objects in a diffuse field. Here we recall how this is determined analytically and approximated numerically. If the ACS of an object under plane-wave illumination by transverse electric (TE) and transverse magnetic (TM) polarized waves from spherical polar direction $(\theta, \varphi)$ are denoted by $\sigma^{\text{TE}}(\theta, \varphi)$ and $\sigma^{\text{TM}}(\theta, \varphi)$ respectively then the AACS for plane-waves arriving from all directions is [8]

$$\langle \sigma^a \rangle = \frac{1}{8\pi} \oiint_{4\pi} \sigma^a_{\text{TE}}(\theta, \varphi) + \sigma^a_{\text{TM}}(\theta, \varphi) \, d\Omega \tag{3}$$

where $d\Omega = \sin\theta \, d\theta \, d\varphi$ is the element of solid angle. A corresponding average absorption efficiency (AAE), $\langle Q^a \rangle$, can be defined by

$$\langle \sigma^a \rangle \overset{\text{def}}{=} \langle Q^a \rangle \langle G \rangle = \tfrac{1}{4} \langle Q^a \rangle A \tag{4}$$

where $\langle G \rangle$ is the average silhouette area of the object, which for a convex object is equal to a quarter of its surface area, $A$.

Equation (3) can be evaluated numerically using Gauss-Legendre quadrature (GLQ) on a sphere [13]: For order $L$ the azimuthal angle is sampled at $\varphi_m = m\pi/L$ ($m = 1, \ldots, 2L$) and the polar angle at $\theta_l$ ($l = 1, \ldots, L$) corresponding to the zeros of the Legendre polynomial of order $L$, $P_L(\cos(\theta_l)) = 0$. The resulting numerical approximation is

$$\langle \sigma^a \rangle = \frac{1}{8L} \sum_{l=1}^{L} \sum_{m=1}^{2L} w_l \big( \sigma^a_{\text{TE}}(\theta_l, \varphi_m) + \sigma^a_{\text{TM}}(\theta_l, \varphi_m) \big) \tag{5}$$

where $w_l$ is the Gauss-Legendre weighting factor. In order to fully sample the potential spatial variation of the fields at wavelength $\lambda$ due to an object of maximum linear size $D$ the order of quadrature must satisfy [14], [15]

$$L \gtrsim \frac{\pi}{\lambda}(D + \lambda) . \tag{6}$$

If $f_{\text{max}}^{\text{GHz}}$ is the desired maximum frequency in gigahertz for the numerical evaluation of the AACS then this can be written

$$L \gtrsim \pi + 10 D f_{\text{max}}^{\text{GHz}} . \tag{7}$$

For planar objects illuminated from one side only (e.g. the walls of an enclosure) the integration in (3) should be restricted to $2\pi$ steradians and the sum over $l$ in (5) limited to those values giving $\cos(\theta_l) \geq 0$. In this case, for odd orders the weight for samples at $\cos(\theta_l) = 0$ should also be halved. This results in an AACS that when multiplied by the average scalar power density in the enclosure gives the power absorbed in walls; the factor of one-half, accounting for the fact that the walls only see a diffuse field coming from a hemisphere, is included in the definition of the AACS.

### C. Lossy dielectric surfaces

The AAE of an infinite sheet of laminated lossy dielectric material backed by a metal plate is given by [3]

$$\langle Q^a \rangle = \frac{1}{\pi} \int_0^{2\pi} \int_0^{\pi/2} T(\theta) \cos\theta \sin\theta \, d\theta d\varphi \tag{8}$$

where

$$T(\theta) = 1 - \frac{1}{2}[|\Gamma^{\text{TE}}(\theta)|^2 + |\Gamma^{\text{TM}}(\theta)|^2] \tag{9}$$

and $\Gamma^{\text{TE}}(\theta)$ and $\Gamma^{\text{TM}}(\theta)$ are the total reflection coefficients of the surface for TE and TM polarised plane-waves with angle of incidence $\theta$. For a laminated surface the total reflection coefficients at the outer surface can be calculated recursively from the material parameters and thickness of each layer [16].

The AACS of a given area of the laminated surface can then be estimated from (4). For a finite sized slab of material, with

length, $l$, width, $w$, and height, $h$, over a metal plate this approach, taking $A = lw$, is expected to provide a good estimate for the AACS if the slab is electrically large and its height is small. If the slab has significant height then it is more appropriate to estimate its AACS using its total exposed surface area, $A = lw + 2h(l + w)$, while retaining the AAE predicted by (8). This is an approximation; however, we will show later that it can still provide a good estimate of the AACS that is suitable for design purposes.

*D. Microstrip transmission lines*

An analytic model for the excitation of a microstrip line by a plane-wave has been derived by Leone and Singer [17]. The expressions for the terminal currents therein can be used to determine the AACS of the loads of a microstrip line in a diffuse field by applying the GLQ approach outlined in Section II-B. This model does not account for dielectric, conductor or radiation losses that become more significant at high frequencies; however, it is still expected to provide a reasonable first-order estimate of the AACS of a microstrip line up to the frequency at which the electrical height of the line becomes comparable to a wavelength. The model has been implemented in a high-level dynamic scripting language and requires about 20 seconds to estimate the AACS of a single line on a desktop computer.

## III. ReCo Design and Fabrication

*A. ReCo specification*

The philosophy of the proposed approach is to match the AACS of ReCos to real PCBs. Since the ReCo has to be installed into the enclosure for the shielding measurement it is natural to require it to have the same dimensions (length, $l_{\mathrm{PCB}}$, and width, $w_{\mathrm{PCB}}$) as the PCB it is a surrogate for. The target AACS for a particular ReCo should be statistically determined from a class of PCBs of similar type and size to those intended to be used in the enclosure. In [10], the AACS of a large sample of PCBs was measured. The corresponding AAE ranged from -19 dB up to -4 dB with a mean of about -8 dB. The range of the AAE from the $10^{\mathrm{th}}$ to $90^{\mathrm{th}}$ percentile was about 6 dB. Equation (1) shows that if, as is likely, $\langle \sigma^{\mathrm{a}}_{\mathrm{i;contents}} \rangle / \langle \sigma^{\mathrm{t}} \rangle \gg 1$ then $\langle SE \rangle \propto \langle \sigma^{\mathrm{a}}_{\mathrm{i;contents}} \rangle$ and any deviation in the AACS of the contents is reflected as the same relative deviation in the SE. For a qualification measurement it may be prudent to choose a target AACS for the ReCos that is lower than the mean of the expected PCB AACS distribution, for example the lower quartile, so that the SE of the enclosure is conservative with regard to the statistical deviations of the contents.

To help quantify the effect of variations in PCB AACS we consider a simple Monte Carlo Model (MCM) of the combined AACS of a number of PCBs. The total AACS of a stack of $N_{\mathrm{PCB}}$ equal sized PCBs is estimated as

$$\langle \sigma^{\mathrm{a}}_{\mathrm{stack}} \rangle = \frac{A_{\mathrm{PCB}}}{4} \sum_{i=1}^{N_{\mathrm{PCB}}} \gamma^i_{\mathrm{shad}} \langle Q^{\mathrm{a}}_i \rangle \qquad (10)$$

where $\langle Q^{\mathrm{a}}_i \rangle$ is a uniformly distributed random variable in the measured range of -10 dB to -4 dB, $A_{\mathrm{PCB}} = 2l_{\mathrm{PCB}} w_{\mathrm{PCB}}$ and
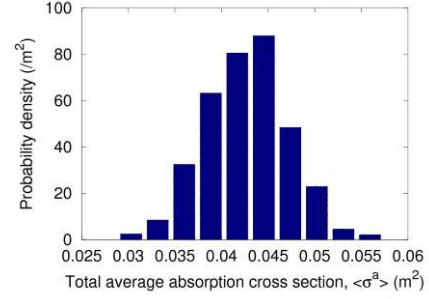


Fig. 1. MCM prediction of the AACS distribution of a stack of twelve PCBs with uniform random distributions of AAE and shadowing factor.
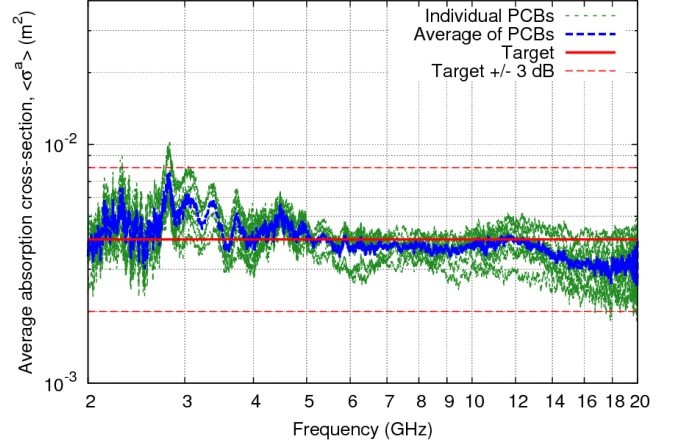


Fig. 2. Measured AACS of the eight PCBs used to determine the target AACS for the ReCo [10]. The average of these AACS is also shown together with the simplified frequency independent "flat target" level of $4 \times 10^{-3}$ m$^2$.

the shadowing factors, $\gamma^i_{\mathrm{shad}}$, are uniformly distributed over the range 0.6 to 0.8 according to the empirical estimates in [10]. Fig. 1 shows the probability density function for the AACS of a stack of twelve PCBs with $l_{\mathrm{PCB}} = 283$ mm and $w_{\mathrm{PCB}} = 144$ mm from fifty runs of the MCM. The coefficient of variation is about 10 %, indicating modest variability. This suggests that using a single ReCo design for all the PCBs in this stack would give a reasonable representation of the overall loading effect of the real PCBs on an enclosure.

For the purposes of illustrating the methodology, in this paper we report the design and fabrication of ReCos to match a subset of the PCBs in [10]. These PCBs all have the same size (283 mm ×144 mm) and form two stacks of four in a 2U ICT rack unit. The PCBs had a range of surface populations and structures, including heatsinks and shielded areas; examples can be seen in [10]. The individual AACSs of all eight PCBs and their average AACS are shown in Fig. 2; the average is relatively flat and mostly in the range $3 \times 10^{-3}$ m$^2$ to $5 \times 10^{-3}$ m$^2$. A simple frequency independent "flat target" of $4 \times 10^{-3}$ m$^2$, equivalent to a two-sided AAE of -7 dB, was therefore used for the ReCo design, with a tolerance of ±3 dB.

*B. RAM based ReCo*

The first approach to developing a ReCo was to extend the ideas from work at low frequencies [6] and use a slab of RAM with dimensions and electrical properties chosen to match the desired AACS. The RAM is placed onto a metal ground plane to replicate that of the PCBs. The initial design was made
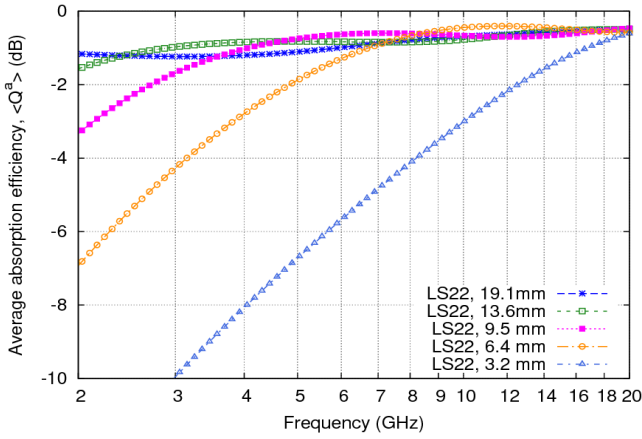
Fig. 3. AAE of various thicknesses of RAM with the same loading over a metal surface predicted by the PWB model.
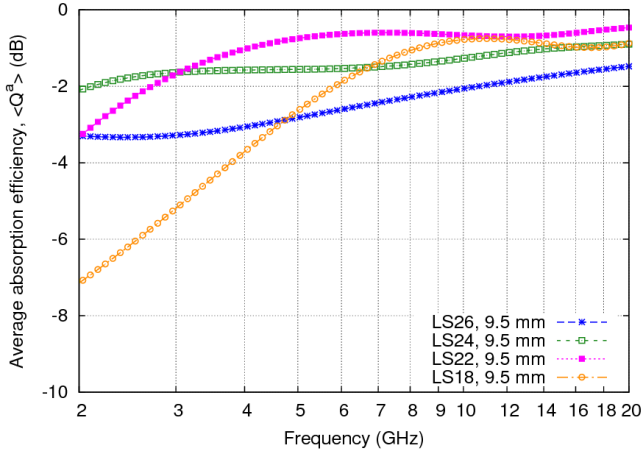


Fig. 4. AAE of different loadings of RAM with the same thickness over a metal surface predicted by the PWB model.

using the PWB model of a laminate presented in Section II-C. According to (4) the AAE of the RAM over the metal plate is the most important design factor.

A range of commercially available carbon-loaded polyurethane foam RAM types were investigated [18]. For each type a three-pole Debye dispersion relationship

$$\hat{\varepsilon}_r = \varepsilon_\infty + \sum_{k=1}^{3} \frac{\Delta\varepsilon_k}{1+j\omega\tau_k} + \frac{\sigma_{DC}}{j\omega\varepsilon_0} \qquad (11)$$

was fitted to the manufacturer's complex permittivity data using a genetic algorithm. Here $\omega$ is the angular frequency, $\varepsilon_0$ the permittivity of free-space and the other fitted parameters are shown in Table I. These parameters were then used to conduct a parametric analysis of the AAE for a single layer of RAM over a metal plate using the model presented in Section II-C.

Figs. 3 and 4 show the predicted AAE for a range of RAM thicknesses and loadings respectively. At high frequencies the AAE is relatively flat; however, at low frequencies the AAE falls as the effective skin depth in the RAM increases. Using RAM with higher carbon loading mitigates this effect, but reduces the flatness of the AACS at higher frequencies. These effects limit the thinness of RAM that can be used while maintaining a relatively flat AACS profile. In real equipment enclosures the PCB spacing can be as low as 20 mm so a two-sided RAM based ReCo is not feasible using these types of
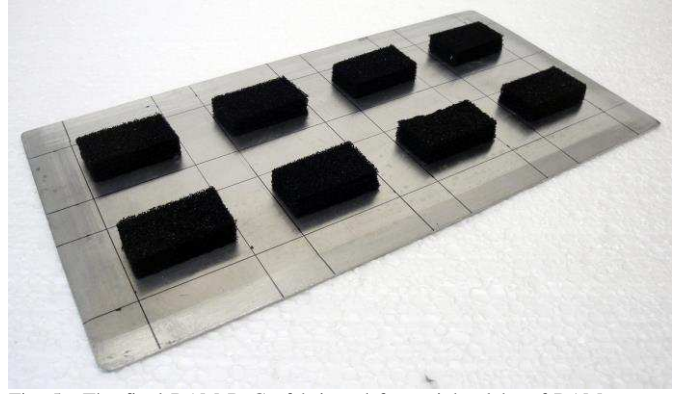


Fig. 5. The final RAM ReCo fabricated from eight slabs of RAM on one side of a metal carrier plate.

TABLE I
THIRD ORDER DEBYE MODELS FOR LS SERIES RAM CARBON LOADED
FOAM, WITH CARBON LOADING INCREASING FROM LEFT TO RIGHT

| Parameter | LS18 | LS22 | LS24 | LS26 |
|---|---|---|---|---|
| $\varepsilon_\infty$ | 1.1686 | 1.1725 | 1.000 | 1.0043 |
| $\Delta\varepsilon_1$ | $2.52\times10^7$ | $1.04\times10^{-3}$ | $3.83\times10^{-3}$ | $1\times10^8$ |
| $\Delta\varepsilon_2$ | 0.626 | 17.9 | 13.9 | 36.2 |
| $\Delta\varepsilon_3$ | 0.107 | 0.490 | 1.50 | 1.98 |
| $\tau_1$ (ms) | 0.997 | 55.3 | 100 | 0.415 |
| $\tau_2$ (ns) | 0.0481 | 0.188 | 0.109 | 0.106 |
| $\tau_3$ (ps) | 4.641 | 6.20 | 5.06 | 3.34 |
| $\sigma_{DC}$ (mS/m) | 89.2 | 0.100 | 0.838 | 0.129 |

RAM. We therefore decided to design a one-sided ReCo with 9.5 mm thick LS22 RAM on one side only, but still matched to the total target AACS of the PCB.

Comparing the target AACS to the appropriate AAE according to (4) suggested that a RAM coverage factor of about 30% is required. For low loss enclosures, full-wave simulations have shown that the statistics of the internal field are independent of the distribution of losses and depend only on the total AACS [19]; however, for higher losses the electromagnetic diffusion model suggests that the diffuse field becomes inhomogeneous and dependent on the loss distribution [20]. The RAM was therefore distributed across the full area of the ReCo by dividing it into eight equal sized slabs. The design was then refined by adjusting the size of the slabs to account for the slab sides as described in Section II-C.

The final design consisted of eight slabs of 9.5 mm high LS22 RAM of dimensions 40 mm × 22.5 mm, spaced at 25 mm along the length and 38 mm across the width of the metal plate. A photograph of the fabricated RAM ReCo is shown in Fig. 5.

### C. Microstrip TL based ReCo

Since the absorption mechanisms for real PCBs are direct absorption in the substrate and component packaging, and indirect dissipation in lumped devices via coupling into transmissions lines, it is natural to consider the development of microstrip TL-based ReCos. For the initial design we considered a one-sided single layer PCB of area $A_{PCB} = l_{PCB}w_{PCB}$ and substrate thickness $h$ with a number of loaded microstrip lines. The total AACS is taken to be composed of parts due to substrate loss and dissipation in the microstrip
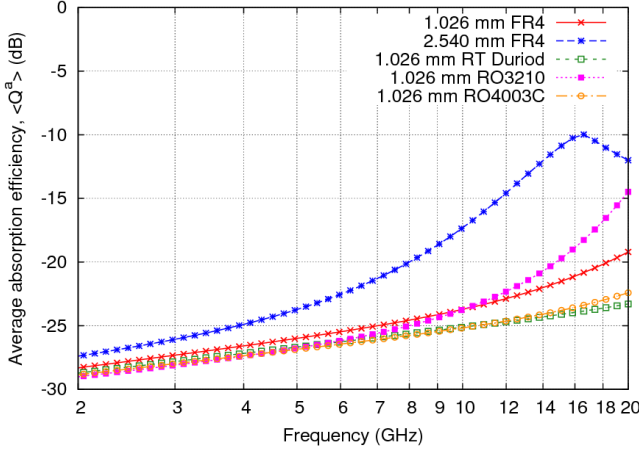
Fig. 6. AACS of infinite planes of different types and heights of PEC-backed substrate material predicted by the PWB model.
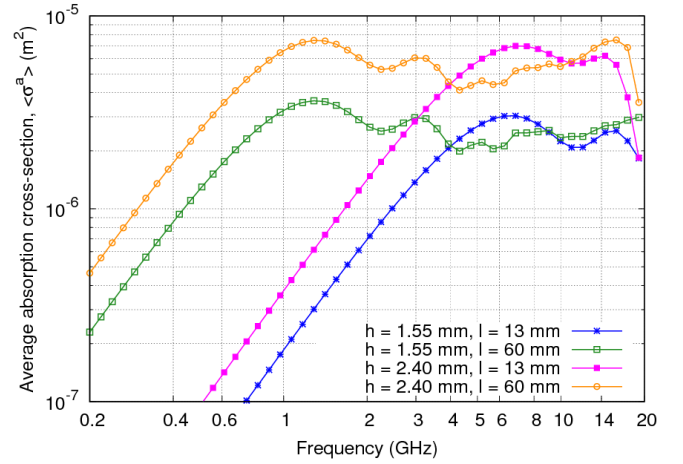


Fig. 7. Effect of substrate height and track length on the AACS of a single matched microstrip line on FR4 substrate predicted by the PWB model.

loads,

$$\langle \sigma^a_{\mathrm{TL}} \rangle = \tfrac{1}{4} \langle Q^a_{\mathrm{sub}} \rangle A_{\mathrm{PCB}} + \langle \sigma^a_{\mathrm{loads}} \rangle \tag{12}$$

where $\langle Q^a_{\mathrm{sub}} \rangle$ is the substrate AAE and $\langle \sigma^a_{\mathrm{loads}} \rangle$ is the total AACS of the loads. Note that we have made the assumption that the two absorption mechanisms are independent, which is an approximation to reality.

We first consider the selection of the substrate material regarding its own losses. Fig. 6 shows the AAE of an infinite single side of a bare substrate (with metal backing) predicted by the PWB model in Section II-C. For FR4, which is not an electrically well-defined material, we have taken the relative permittivity to be $\varepsilon_r = 4.2$ and loss tangent as $\tan \delta = 0.01$. For the other substrates we have used the manufacturers' datasheet values for the complex permittivity (RT Duroid: $\varepsilon_r = 1.96$, $\tan \delta = 0.002$; RO3210: $\varepsilon_r = 10.8$, $\tan \delta = 0.0027$; RO4003C: $\varepsilon_r = 3.38$, $\tan \delta = 0.0025$). Note that the frequency of the substrate thickness resonance, as determined by the relative permittivity, has a significant effect on the ordering of the AAEs at gigahertz frequencies.

These results suggest that the low loss substrates will give an AACS far below the target AACS and the substrate loss can therefore be neglected in the design (at least in so far as the PWB analysis is able to determine). For FR4 the substrate loss will however increase to significant levels relative to the target at high frequencies on thicker substrates. Thicker substrates also increase the loss in the TL loads as we will see below. Since there is no strong indication in the measured AACSs of real PCBs of a rapidly rising AACS with frequency, this potentially makes the design using FR4 more complicated. Nevertheless, FR4 is more representative of the substrates used in typical ICT equipment PCBs, so here we have chosen to develop TL ReCos using it.

In the PWB model we assume that microstrip lines absorb independently so that the overall AACS of $N_t$ straight tracks on a substrate of height $h$ and complex relative permittivity $\hat{\varepsilon}_{r;\mathrm{sub}}$ is

$$\langle \sigma^a_{\mathrm{tracks}} \rangle = \sum_{i=1}^{N_t} \langle \sigma^a_j \big( h, \hat{\varepsilon}_{r;\mathrm{sub}}, l_j, w_j, Z_{1;j}, Z_{2;j} \big) \rangle \tag{13}$$

where $\langle \sigma^a_j \big( h, \hat{\varepsilon}_{r;\mathrm{sub}}, l_j, w_j, Z_{1;j}, Z_{1;j} \big) \rangle$ is the AACS of the $j$-th
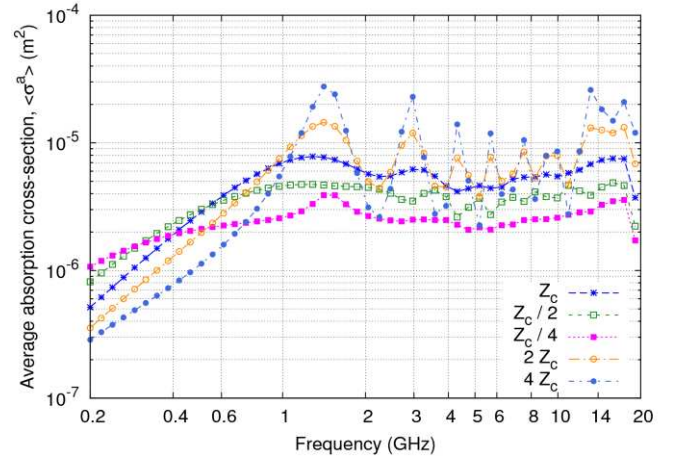


Fig. 8. Effect of mismatch on the AACS of a single 60 mm long 100 Ω line on 2.4 mm FR4 substrate predicted by the PWB model.

track, which has length $l_j$, width $w_j$ and load impedances $Z_{1;j}$ and $Z_{2;j}$. The assumption of independent absorption will clearly become more approximate as the tracks are placed closer together.

A parametric analysis of the AACS of a single track on FR4 substrate was carried out from 0.2 to 20 GHz using the numerically integrated Leone and Singer PWB microstrip model from Section II-D. Fig. 7 shows the results for "short" (13 mm) and "long" (60 mm) tracks of width 1 mm on two substrate heights. Shorter tracks (less than a fifth of a wavelength) lead to a decrease in AACS, while tracks longer than a couple of wavelengths do not give any enhancement in AACS. Fig. 8 shows the effect on the AACS of the track termination impedance (the same at both ends) for a 100 Ω track on 2.4 mm FR4. Mismatch generally increases the frequency variation in the AACS. The model can be seen to break down at about 16 GHz, when the electrical height of the line is a quarter of a wavelength.

Fig. 7 and Fig. 8 show that a single track has a significantly frequency-dependent AACS. In order to achieve the relatively flat response of the target AACS we therefore chose to use a large collection of tracks with different lengths. Further, the "ripple" due to moderate mismatches ($Z_{1,2} \sim 2Z_c$) is also
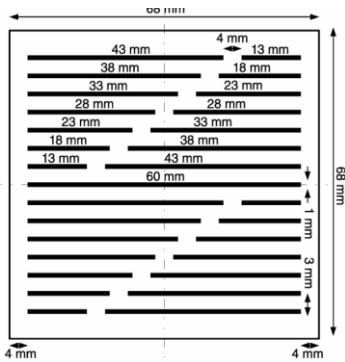
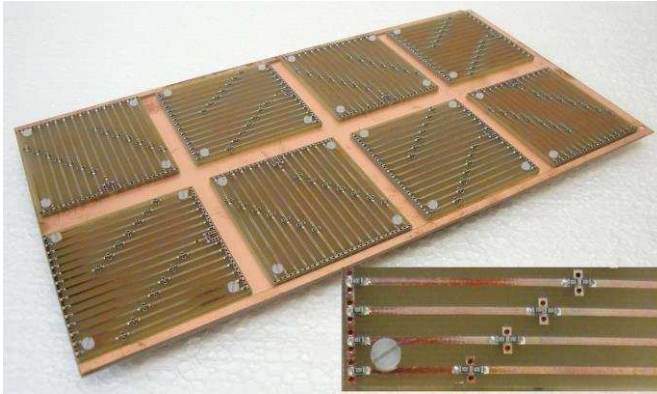Fig. 9. The 29 track unit cell design of the TL ReCo.



Fig. 10. The final TL ReCo consisting of 16 unit cells of 29 tracks, with 8 cells mounted on each side of a double sided PCB carrier board. Note that the notch near one end of the central track on each cell is to allow the connection of a 50 Ω RG-405/U semi-rigid cable to monitor the power. The inset shows the detail of the surface mount terminating resistors. Pads with three vias were used to reduce the parasitic inductance.
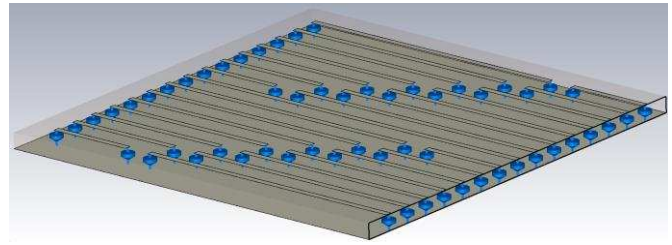


Fig. 11. Full-wave simulation model of the TL ReCo unit cell with the substrate shown as translucent so that the thin wires with lumped loads (blue discs) used to terminate the tracks can be seen.

averaged out by using tracks of different length, yielding a higher AACS than for matched lines while still maintaining a relatively flat frequency spectrum. A simple MCM of (13) was used to estimate the number of 1 mm wide tracks required to achieve the target AACS on 2.4 mm FR4, taking the track lengths from a uniform distribution over the interval 13 mm to 60 mm. We found that about 470 tracks are necessary.

The final design used 464 tracks of width 1 mm on 2.4 mm FR4 with 200 Ω terminating surface mount resistors (twice the characteristic impedance). Rather than use a completely random distribution of tracks, from the perspective of eventual standardization and modularization of the ReCo, it was desirable to partition the tracks into a number of identical square "unit cells". We therefore designed the ReCo using 16 unit cells (8 per side). The unit cell, shown in Fig. 9, consists of 29 tracks with 8 different lengths. The arrangement of the unit cells on each side of the ReCo is shown in the photograph of one of the fabricated surrogates in Fig. 10. Note that the orientation of the cells alternates in order to randomize the absorption of different polarizations of the field.

## IV. FULL-WAVE SIMULATIONS

To verify the ReCo designs full-wave simulations of both the RAM and TL ReCos were undertaken using the Finite Integration Technique (FIT) solver of CST Microwave Studio [21]. The diffuse environment was modeled by illuminating the ReCos with a number of plane-waves, with arrival angles chosen according to the GLQ approximation in (5) and two orthogonal polarization angles for each set of arrival angles.

The estimate for the order of GLQ required to achieve convergence at 20 GHz given by (7) is far too high for practical FIT simulations. We therefore tested the convergence of the AACS predicted by the microstrip PWB model of the unit cell with the order of GLQ and found that 32 plane-wave directions (64 plane-waves in total) was sufficient to achieve an AACS within ±1 dB of the fully converged result. We therefore used 64 plane-waves in the FIT simulations.

For the TL ReCo only one unit cell was simulated above an effectively infinite substrate and ground plane, as shown in Fig. 11. The overall AACS of the TL ReCo was then estimated by assuming the AACS of the unit cells is additive. The infinite substrate was modeled by placing perfectly matched layer (PML) boundary conditions along the edges of the unit cell with the ground plane forming the lower boundary of the computational mesh and a further PML placed half a wavelength from upper surface of the substrate at the lowest frequency of the simulation. This effectively reduces the problem to a half-space and means that in fact only 32 plane-waves needed to be simulated.

The ground plane and tracks were modeled as perfect electric conductor (PEC) surfaces and the substrate as either a lossless dielectric with a frequency independent relative permittivity of 4.2 or as a lossy dielectric with an additional loss tangent of 0.01. The terminations were modeled as thin wires with lumped resistive loads. The edge lengths of the non-uniform computational mesh ranged from 0.12 mm to 1.48 mm, giving a total of about 5.5 million cells. The lossless substrate simulation required about 4 minutes per plane-wave to run on 10 cores of a 2.8 GHz Intel Xeon E5-2680 v2 CPU.

For the RAM ReCo the full ReCo was included in the simulation with the ground plane again modeled as a PEC surface and the RAM slabs as lossy dielectrics using the dispersion relationship defined in (11) with the parameters given in Table I. PML boundary conditions were applied in all directions at a separation of half a wavelength from the structure at the lowest frequency of the simulation. This model had a total of about 9 million cells and the simulation took about 12 minutes per plane-wave to run on a 3.2 GHz Intel Core i7 CPU.
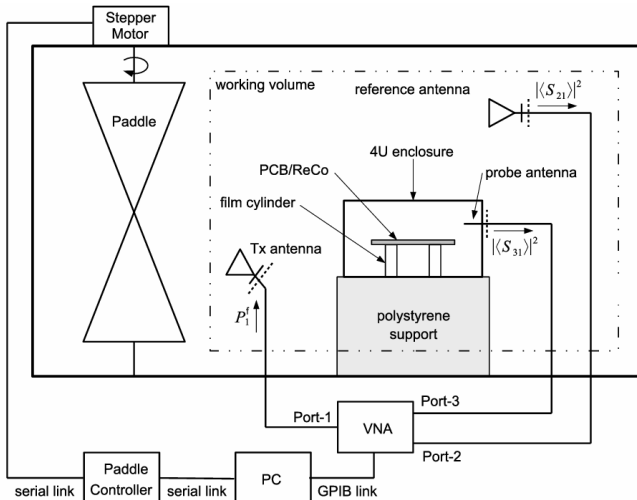
Fig. 12. SE measurement configuration in the RC.

## V. VALIDATION MEASUREMENTS

To verify that the designs of the ReCos achieved the specified target their AACSs were measured in an RC of dimensions 0.6 m × 0.7 m × 0.8 m using exactly the same methodology and parameters as described in [10]. In brief, the mismatch corrected insertion loss between two monopole antennas in the chamber was measured, both with and without the ReCo inside. The additivity of AACS then allows the AACS of the ReCo to be determined from the average power balance of the chamber [11].

To validate the effectiveness of the ReCos at replicating the environment inside a loaded enclosure we then measured the SEs of a commercial 4U 19-inch rack unit enclosure of internal dimensions 170 mm × 405 mm × 455 mm containing both the real PCBs and ReCos. The enclosure had perforated ventilation apertures on the top and bottom walls and a nominal "SE" of 30 dB at 1 GHz according to the manufacturer's datasheet.

The measurements were made in an RC of dimensions 4.7 m × 3.0 m × 2.37 m according to the IEEE299.1 standard [7]. The measurement configuration is shown in Fig. 12. Very thin plastic films formed into two cylinders of diameter 20 mm were used to support the PCB/ReCo near the center of the enclosure with no "ground" connection to the enclosure. Since the PCB/ReCo was at least half a wavelength from the enclosure wall over the measurement band and its AACS represented relatively light loading of the enclosure its exact location does not significantly influence the SE. The enclosure was illuminated using a double ridged waveguide horn antenna (port-1) and the field in the working volume was monitored using a similar antenna (port-2). A top-loaded monopole probe (port-3) of length 20 mm with a 60 mm diameter circular ground plane was used to monitor the internal field. The average SE was determined using [7]

$$\langle SE \rangle = \frac{\langle |s_{21}|^2 \rangle}{\langle |s_{31}|^2 \rangle} \cdot \frac{1 - |\langle s_{33} \rangle|^2}{1 - |\langle s_{22} \rangle|^2} \qquad (14)$$

where $S_{ij}$ is the complex scattering parameter from port-$j$ to port-$i$, as measured using a vector network analyzer.
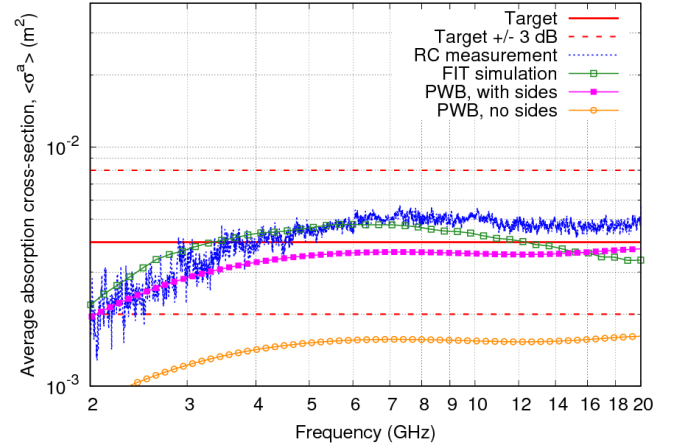


Fig. 13. AACS of the RAM ReCo measured in the RC compared to the nominal target, the FIT simulation result and PWB model predictions with and without the side area of the RAM slabs included.
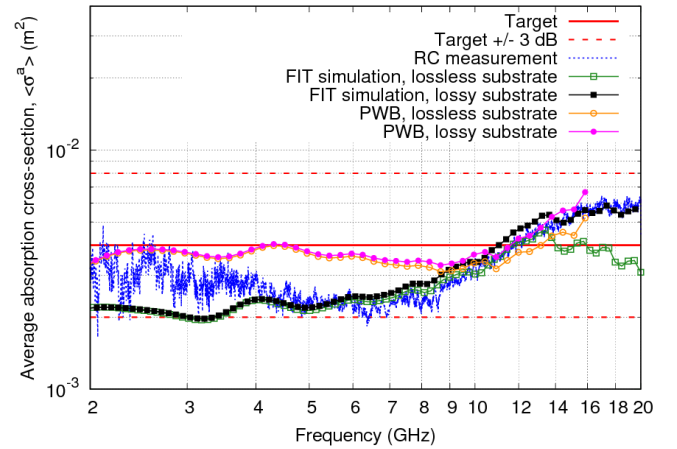


Fig. 14. AACS of the TL ReCo measured in the RC compared to the nominal target, the FIT simulation results and PWB model predictions. The PWB results are only shown to 16 GHz, where the model breaks down.

Data was collected for 100 paddle positions at 10,001 frequency points over the 2-20 GHz band and frequency stirring applied over a 100 MHz bandwidth.

## VI. RESULTS

### A. ReCo AACS

The measured AACS of the RAM ReCo is shown in Fig. 13, compared to the target, PWB predictions and FIT simulation result. The measured AACS is within the target range over the whole band and is in good agreement with the FIT simulation and the PWB prediction that uses the total exposed area of the RAM. The PWB model using only the top surface area can be seen to significantly underestimate the AACS. The greatest deviation of the measured AACS from the target is at the lower frequencies, where the skin depth is comparable to the RAM height, causing the AACS to drop.

Fig. 14 shows show the measured AACS of the TL ReCo compared to the PWB model and FIT simulation results. The AACS is again within the target range with a deviations of up to -3/+2 dB. The PWB model prediction is within about 2 dB of the measured result; it overestimates the AACS below 10 GHz, presumably due to the fact it does not account for the
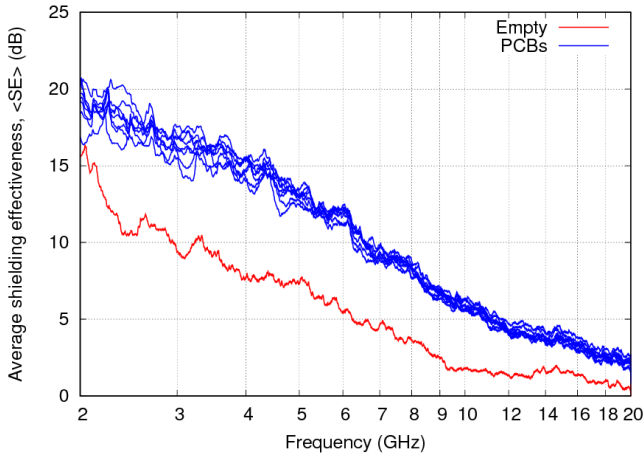
Fig. 15. Measured average SE of the empty enclosure and the enclosure populated with each of the eight real PCBs.
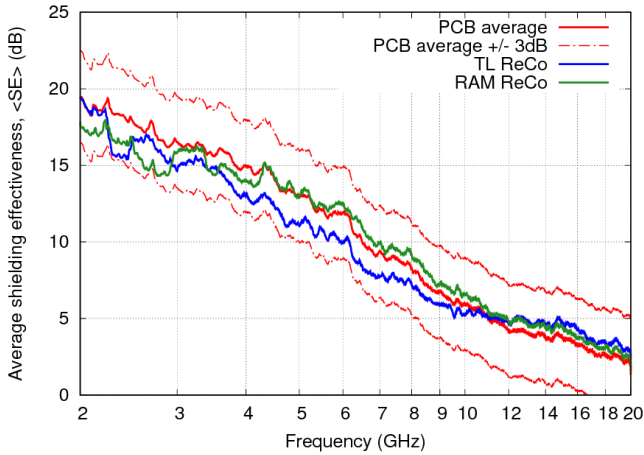


Fig. 16. Measured average SE of the enclosure populated with RAM and TL ReCos compared to the average SE when populated with the real PCBs.



Fig. 17. Average SE of the enclosure populated with the RAM and TL ReCos predicted from their measured AACSs and the SE of the empty enclosure compared to the corresponding directly measured average SEs.

Finally we investigated the validity of (2) for predicting the average SE of the enclosure. In order to estimate the ATCS a cube of RAM with known AACS, $\langle \sigma_{i;cube}^{a} \rangle$ (see **Error! Reference source not found.**), was placed inside the enclosure and the SE measured. Equation (1) was then used to determine $\langle \sigma^{t} \rangle$ under the assumption that $\langle \sigma_{i;walls}^{a} \rangle \ll \langle \sigma_{i;cube}^{a} \rangle$. The SE of the enclosure populated with the RAM ReCo and TL ReCo was then estimated from (2) using this ATCS and the measured AACSs of the ReCos. The results are shown in Fig. 17, compared to the directly measured SEs. The predicted SEs are in excellent agreement with the directly measured ones across the whole frequency band.

## VII. CONCLUSIONS

The SE of a populated enclosure depends on the losses in the enclosure contents. We have shown that AACS can be used to match the loading effect of real enclosure contents, such as PCBs, to surrogate ReCos at high frequencies. To practically demonstrate this, both RAM and microstrip TL based ReCos, matched to PCBs from an ICT enclosure, were successfully designed using PWB models and verified by full-wave simulations over the frequency range 2-20 GHz. The ReCos were fabricated and their designs validated by measuring their AACSs and comparing them to the real PCBs. The validity of the ReCos as surrogates in shielding measurements was further validated by comparing the measured SE of an enclosure populated with the real PCBs to that populated with the ReCos. The ReCos were found to perform as expected, giving the same SE as the original PCBs, within the deviations of the ReCo AACSs from that of the PCBs. Furthermore, we have shown that the SE of a populated enclosure can be accurately predicted from the AACS of the contents if the ATCS of the enclosure is known, at least in the case of low population density in the enclosure. The ATCS of an enclosure is therefore an equally useful metric as the unpopulated SE at high frequencies.

The methodology presented is the foundation of an approach to the high frequency qualification of enclosures using generic contents that is readily amenable to

screening effect of closely spaced lines. The FIT simulations are in very good agreement with the measurement and demonstrate the increasing absorption in the substrate above 12 GHz. The deviation of the FIT results from the measurements below 4 GHz is caused by the use of an infinite, rather than a finite sized, ground plane in the simulation.

### B. Enclosure SE

The measured average SEs of the 4U enclosure when empty and when populated with each of the real PCBs are shown in Fig. 15. This figure shows that the contents contribute significantly to the SE at all frequencies and are the dominant contributor to lowering the average internal power density at high frequencies. The eight PCBs had similar AACSs so the SEs with the PCBs are also quite similar according to (2).

Fig. 16 shows the SE of the enclosure populated with the RAM and TL ReCos compared to the (linear) average SE measured with the real PCBs. The SE with the real contents and ReCos are in very good agreement. The deviation between the SEs with the PCBs and ReCos is almost entirely explained by the deviations between the ReCo AACSs and those of the PCBs: Where the ReCo ACS is below the target the SE is underestimated by the same factor and where ReCo ACS is above the target the SE is similarly overestimated.
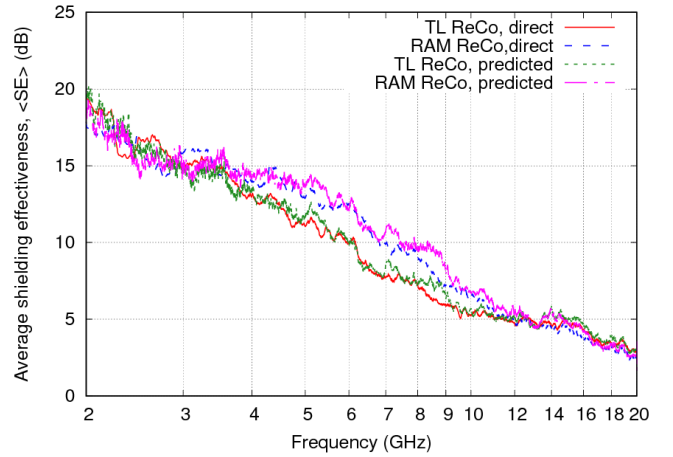
standardization. Further work is continuing to apply more sophisticated optimization-based techniques to the design of both RAM and TL ReCos. The effect of shadowing in more densely populated enclosures is also under investigation.

## REFERENCES

[1] D. W. P. Thomas, A. Denton, T. Konefal, T. M. Benson, C. Christopoulos, J. F. Dawson, A. C. Marvin and S. J. Porter, "Characterisation of the shielding effectiveness of loaded equipment enclosures," *in Proc. Int. Conf. Exhibit. Electromagn. Compat. (EMC York 99)*, York, UK, Jul. 12-13, 1999, pp. 89–94.

[2] A. Lozano, M. P. Robinson, A. Díaz and J. V. Balbastre, "Evaluation and optimization of an equivalent model for printed circuit boards inside metallic enclosures," *in Proc. XXIX General Assembly Int. Union Radio Sci. (URSI)*, Chicago, IL, Aug. 7-16, 2008, paper no. EBp6.

[3] A. Gifuni, "Relation between the shielding effectiveness of an electrically large enclosure and the wall material under uniform and isotropic field conditions," *IEEE Trans. Electromagn. Compat.*, vol. 55, no. 6, pp. 1354-1357, Dec. 2013.

[4] I. J. Washbourne, V. Rajamani, C. F. Bunting, J. C. West, B. Archambeault and S. Connor, "Effectiveness of absorbing materials on reducing electromagnetic emissions from cavities measured using a nested reverberation chamber approach," *in Proc. IEEE Int. Symp. Electromagn. Compat.*, Raleigh, NC, August 4-8, 2014, pp. 909-912.

[5] A. C. Marvin and Y. Cui, "Towards evaluating the shielding of enclosures with contents at frequencies above 1 GHz," *in Proc. IEEE Int. Symp. Electromagn. Compat.*, Chicago, IL, Aug. 8-12, 2005, pp. 200-205.

[6] A. C. Marvin, J. F. Dawson, S. Ward, L. Dawson, J. Clegg and A. Weissenfeld, "A proposed new definition and measurement of the shielding effect of equipment enclosures," *IEEE Trans. Electromagn. Compat.*, vol. 46, no. 3, pp. 459-468, Aug. 2004.

[7] IEEE-STD 299.1, "Standard method for measuring the shielding effectiveness of enclosures and boxes having all dimensions between 0.1 m and 2 m," *Institute of Electrical and Electronics Engineers*, Piscataway, NJ, October 2013.

[8] D. A. Hill, M. T. Ma, A. R. Ondrejka, B. F. Riddle, M. L. Crawford and R. T. Johnk, "Aperture excitation of electrically large, lossy cavities," *IEEE Trans. Electromagn. Compat.*, vol. 36, no. 3, pp. 169-178, Aug. 1994.

[9] I. Junqua, J.-P. Parmantier and F. Issac, "A network formulation of the power balance method for high-frequency coupling," *Electromagnetics*, vol. 25, no. 7-8, pp. 603-622, 2005.

[10] I. D. Flintoft, S. L. Parker, S. J. Bale, A. C. Marvin, J. F. Dawson and M. P. Robinson, "Measured average absorption cross-sections of printed circuit boards from 2 to 20 GHz," *IEEE Trans. Electromagn. Compat.*, vol. 58, no. 2, pp. 553-560, Apr. 2016.

[11] U. Carlberg, P.-S. Kildal, A. Wolfgang, O. Sotoudeh, and C. Orlenius, "Calculated and measured absorption cross sections of lossy objects in reverberation chamber," *IEEE Trans. Electromagn. Compat.*, vol. 46, no. 2, pp. 146–154, May 2004.

[12] A. C. Marvin, J. F. Dawson, S. Ward, L. Dawson, J. Clegg, and A. Weissenfeld, "A proposed new definition and measurement of the shielding effect of equipment enclosures," *IEEE Trans. Electromagn. Compat.*, vol. 46, no. 3, pp. 459-468, Aug. 2004.A. Gifuni, A. Sorrentino, A. Fanti, G. Ferrara, M. Migliaccio, G. Mazzarella and F. Corona, "On the evaluation of the shielding effectiveness of an electrically large enclosure," *Adv. Electromagnetics*, vol. 1, no. 1, pp. 84-91, May 2012.

[13] K. Atkinson, "Numerical integration on the sphere," *J. Austral. Math. Soc. (Series B)*, vol. 23, pp. 332-334, 1982.

[14] O. M. Bucci, C. Gennarelli and C. Savarese, "Optimal interpolation of radiated fields over a sphere," *IEEE Trans. Antennas Propagat.*, vol. 39, no. 11, pp. 1633-1643, Nov. 1991.

[15] J. C. West, C. F. Bunting and V. Rajamani, "Accurate and efficient numerical simulation of the random environment within an ideal reverberation chamber," *IEEE Trans. Electromagn. Compat.*, vol. 54, no. 1, pp. 167-173, Feb. 2012.

[16] S. J. Orfanidis, *Electromagnetic waves and antennas*, Piscataway, NJ, USA: Rutgers University, 2016. [Online] http://www.ece.rutgers.edu/~orfanidi/ewa.

[17] M. Leone and H. L. Singer, "On the coupling of an external electromagnetic field to a printed circuit board trace," *IEEE Trans. Electromagn. Compat.*, vol. 41, no. 4, pp. 418-424, Nov. 1999.

[18] Eccosorb LS Series Microwave Absorber, Emerson and Cuming Microwave Products Inc. URL: http://www.eccosorb.com.

[19] F. Moglie, L. Bastianelli and V. M. Primiani, "Reliable finite-difference time-domain simulations of reverberation chambers by using equivalent volumetric losses," *IEEE Trans. Electromagn. Compat.*, vol. 58, no. 3, pp. 653-660, Jun. 2016.

[20] I. D. Flintoft, A. C. Marvin, F. I. Funn, L. Dawson, X. Zhang, M. P. Robinson and J. F. Dawson, "Evaluation of the diffusion equation for modeling reverberant electromagnetic fields," *IEEE Trans. Electromagn. Compat.*, vol. 59, no. 3, pp. 760-769, Jun. 2017.

[21] Microwave Studio, Computer Simulation Technology (CST) AG. URL: https://www.cst.com.

[22] I. D. Flintoft, S. J. Bale, S. L. Parker, A. C. Marvin, J. F. Dawson and M. P. Robinson, "On the measureable range of absorption cross-section in a reverberation chamber," *IEEE Trans. Electromagn. Compat.*, vol. 58, no. 1, pp. 22-29, Feb. 2016.